



Cite this: *Dalton Trans.*, 2019, **48**, 17874

In situ synthesis of CuO nanoparticles over functionalized mesoporous silica and their application in catalytic syntheses of symmetrical diselenides†

Trisha Das, ^a Rana Chatterjee, ^b Adinath Majee, ^b Hiroshi Uyama, ^c David Morgan ^d and Mahasweta Nandi *^a

A versatile and novel catalyst, CuO nanoparticles immobilized over functionalized mesoporous silica (**nCuO-FMS**), has been synthesized over an organically modified mesoporous silica framework following a facile synthetic route. The surface of the silica support (SBA-15) is first grafted with the 3-aminopropyl silane group and then further functionalized with tris(4-formylphenyl)amine. The reaction is performed in such a way that a few –CHO groups remain free for further functionalization. Finally, the CuO nanoparticles immobilized on mesoporous silica are obtained by a one pot reaction between the functionalized silica, 2-aminophenol and CuCl₂. The product obtained has been used as a catalyst for the syntheses of symmetrical diselenides in the presence of KOH as the base and dimethyl sulphoxide (DMSO) as the solvent. The materials have been characterized thoroughly by X-ray powder diffraction, nitrogen adsorption–desorption studies, transmission electron microscopy, thermal analysis and different spectroscopic techniques. The Cu content of the sample has been determined by atomic absorption spectrophotometry (AAS). The products of the catalytic studies have been identified and estimated by NMR spectroscopy. Almost 78% isolated yield could be achieved at 363 K within 3 hours of the reaction and the catalyst, **nCuO-FMS**, can be recycled at least up to five catalytic cycles.

Received 21st August 2019,
Accepted 18th November 2019

DOI: 10.1039/c9dt03418h

rs.c.li/dalton

Introduction

It is known that metal containing heterogeneous catalysts are advantageous over their homogeneous counterparts due to multiple reasons like recyclability, easy recovery and high surface accessibility and are often economical with respect to conventional catalysts which can be used only once. However, leaching is a typical problem for heterogeneous catalytic systems and in such cases it becomes difficult to ascertain whether the metal ion bound to the solid support or the metal ion leached into the solution is responsible for catalyzing the

reaction. To overcome this problem, the metal ion should strongly interact with the heterogeneous support so that it does not get detached from the solid framework during the liquid phase catalytic process. Different types of solid supports *e.g.* polymers,¹ zeolite,² alumina,³ silica,⁴ graphene,⁵ mesoporous carbon,⁶ carbon nanotubes,⁷ metal–organic frameworks,⁸ metal oxide nanoparticles,⁹ *etc.*^{10–12} have been used for the successful syntheses of heterogeneous catalysts. Among these, mesoporous silica is often chosen as the solid support because of its better interaction with the metal centers and accessibility to the substrates. These take place due to its large surface area¹³ which significantly increases the efficiency of the catalysts. Apart from this, it is also possible to tune the pore size of the mesoporous silica matrix as per the specific requirements. Silicate-based structures are generally robust, and thermally and chemically stable. Functionalization of their framework can be done easily to introduce hydrophobicity through the insertion of various organic moieties. Moreover, if such organic functionalities are heteronuclear molecules, then various heteroatoms like N, O and S can be introduced into the materials, taking into account their advantage. The introduction of such groups can modify the affinities

^aIntegrated Science Education and Research Centre, Siksha Bhavana, Visva-Bharati University, Santiniketan 731 235, India.

E-mail: mahasweta.nandi@visva-bharati.ac.in

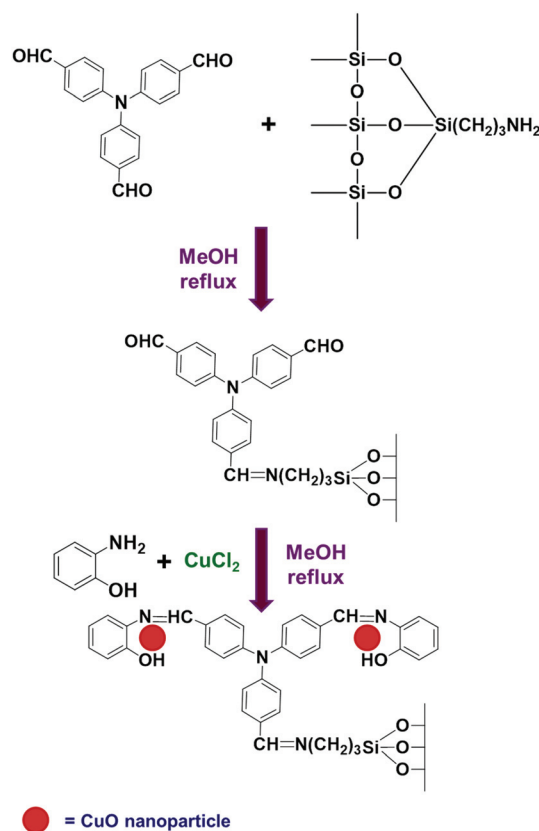
^bDepartment of Chemistry, Siksha Bhavana, Visva-Bharati University, Santiniketan 731235, India

^cDepartment of Applied Chemistry, Graduate School of Engineering, Osaka University, 2-1 Yamadaoka, Suita, Osaka, 565-0871, Japan

^dCardiff Catalysis Institute, School of Chemistry, Cardiff University, Park Place, Cardiff CF10 3AT, UK

†Electronic supplementary information (ESI) available. See DOI: 10.1039/C9DT03418H

Organochalcogen compounds are known to function as biologically active molecules^{24,25} and have been used as reaction intermediates and reagents in various organic syntheses.^{26–28} Apart from these, the organoseleno compounds have found important applications as antioxidants, anti-ulcer and anti-inflammatory agents.^{29–31} Several organoseleno compounds have been used as therapeutic agents in the treatment of cancer and various infectious diseases and as apoptosis inducers.^{32,33} These compounds also play a vital role in the fields of materials science and nanotechnology.^{34,35} Owing to such immense contribution of the organoseleno compounds (especially the diselenides) across several fields of application, there is considerable demand for the preparation of these compounds both in academia and industry. Accordingly, several methods have been developed for the synthesis of diselenide compounds.^{36–43} Among these, a method developed by Braga *et al.* is particularly interesting where diselenide compounds have been synthesized using powder CuO nanoparticles as a catalyst.⁴⁴ In line with this, we have tried to design a mesoporous silica based heterogeneous catalyst containing immobilized CuO nanoparticles instead of the commercially available CuO nanoparticle powder to perform catalytic reactions leading to the formation of diselenides. We have prepared CuO nanoparticles immobilized over functionalized mesoporous silica (**nCuO-FMS**) through a one-pot synthetic



Scheme 1 Synthesis of nCuO-FMS.

strategy (Scheme 1). The CuO nanoparticles are spontaneously formed *in situ* under the reaction conditions in the presence of *tris*(4-formyl phenyl)amine grafted mesoporous silica, 2-aminophenol and CuCl₂. **nCuO-FMS** has been used as a catalyst for the cost effective synthesis of diselenide compounds, including diaryl diselenides. It could be established that the presence of a catalytic amount of this CuO nanoparticle-based catalyst highly influences the progress of the reaction, whereas in the absence of the catalyst the reaction does not proceed. To the best of our knowledge, this is the first report of a CuO nanoparticle based heterogeneous catalyst for the syntheses of diselenides using a neat, facile and innovative technique.

Experimental details

Materials and physical measurements

All the chemicals used in the synthesis have been obtained from commercial sources and used without further purification. The FT-IR spectra of the samples have been collected on a PerkinElmer Spectrum Two spectrometer using the attenuated total reflectance (ATR) method. Thermogravimetric analyses (TGA) have been performed under N₂ atmosphere (flow rate: 50 cc min⁻¹) from room temperature to 1073 K (at heating rate of 2 K min⁻¹) using a PerkinElmer STA-6000

thermal analyzer. Low and high angle powder X-ray diffraction patterns of the samples have been collected on a Bruker D-8 Advance diffractometer using Ni-filtered Cu-K α radiation ($\lambda = 1.5406 \text{ \AA}$) at 40 kV and 40 mA. N₂ sorption isotherms of the samples have been measured using a NOVA 2200e Surface Area and Pore Size Analyzer, Quantachrome Instruments, USA at 77 K. Before performing the measurements, the samples have been degassed for 8–12 h at 353, 393 or 423 K depending on the nature of the samples and the specific surface areas have been obtained by using the Brunauer–Emmett–Teller (BET) method. For obtaining the pore size distributions, the non-local density functional theory (NLDFT) model has been used. The transmission electron microscopic (TEM) images have been recorded on a JEOL JEM-1400 transmission electron microscope. The sample grids for TEM have been prepared by putting one drop of the dispersion of the samples in ethyl alcohol on an amorphous carbon coated copper grid of 400 mesh. Solid state ¹³C CP and ²⁹Si MAS NMR spectra have been recorded on a CHEMAGNETICS 300 MHz CMX 300 spectrometer. A Kratos Axis Ultra DLD system has been used to collect X-ray photoelectron spectra (XPS) using a monochromatic Al K α X-ray source operating at 120 W (10 mA \times 12 kV). Data have been collected with pass energies of 160 eV for survey spectra and 20 eV for the high-resolution scans with step sizes of 1 eV and 0.1 eV, respectively. The system has been operated in the Hybrid mode, using a combination of magnetic and electrostatic lenses and acquired over an area of approximately 300 \times 700 μm^2 . A magnetically confined charge compensation system has been used to minimize the charging of the sample surface, and all the spectra have been recorded with a 90° take off angle. A base pressure of *ca.* 1 \times 10^{−9} Torr has been maintained during the collection of the spectra. Data have been analysed using CasaXPS (v2.3.23) after the subtraction of a Shirley background and using modified Wagner sensitivity factors as supplied by the manufacturer. Atomic absorption spectrophotometric (AAS) studies have been carried out by using a PinAAcle 900F, PerkinElmer atomic adsorption spectrometer. For preparing the sample solution, 0.04 g of **nCuO-FMS** has been dispersed in 2 ml of DTPA (diethylenetriaminepentaacetic acid) solution and the volume has been made up to 20 ml by the addition of distilled water. Then the solution has been shaken for 2 hours and filtered to obtain a colorless filtrate and this filtrate has been used for the analysis. ¹H NMR spectra have been collected in a CDCl₃ solvent using a 400 MHz Bruker spectrometer with tetramethylsilane ($\delta = 0$) as the internal standard. The chemical shifts have been expressed in parts per million (δ). Mass spectra have been obtained by using a Thermo ISQ QD EI Gas Chromatograph-Mass Spectrometer (GC-MS) System.

Synthesis of **nCuO-FMS**

Mesoporous silica, SBA-15, was used as the solid support for the preparation of the **nCuO-FMS** catalyst. For the synthesis of SBA-15,⁴⁵ 1.7 g of Pluronic P123 (poly(ethylene glycol)-*block*-poly(propylene glycol)-*block*-poly(ethylene glycol) *block* copolymer) was taken in a polypropylene bottle and 62 ml of water

was added to it. The mixture was vigorously stirred until all the P123 dissolved and a clear solution was obtained. Then 6 g of 35% HCl solution was added to the mixture and kept again under stirring for 15 min. Finally, 3.5 g of tetraethyl orthosilane was added dropwise to the resulting clear solution and the reaction mixture was stirred for another 20 h at 313 K. The resulting white gel was heated at 373 K for 20 h without stirring in the polypropylene bottle under air-tight conditions. Then the white mixture was cooled to room temperature, filtered and washed with water several times followed by 2–3 washings with ethyl alcohol. The white product was dried under vacuum and then calcined at 773 K for 10 hours in a flow of air to obtain the mesoporous SBA-15.

In the next step, 3-aminopropyl units were grafted onto the surface of SBA-15 by stirring 1.0 g of the mesoporous silica with 1.5 g of 3-aminopropyl triethoxy silane (3-APTES) overnight in chloroform at room temperature under N₂ atmosphere. The mixture was then filtered and the product was washed repeatedly with chloroform and then dichloromethane. Finally, –NH₂ functionalized SBA-15 was obtained after drying the product under vacuum. Further modification of the amine functionalized silica was carried out with *tris*(4-formyl phenyl)amine, a trialdehyde (Scheme 1), which was prepared through the Vilsmeier–Haack formylation reaction of triphenylamine and phosphorus oxychloride following a reported procedure.⁴⁶ In this step, the trialdehyde and the –NH₂ functionalized SBA-15 were refluxed for 4 h in methanol and the molar ratio was kept at 1 : 1, so that two –CHO groups of the trialdehyde remain free for further functionalization.⁴⁷ The resulting light yellow coloured product was filtered and washed repeatedly with methanol until the filtrate became colourless.

For synthesizing **nCuO-FMS**, the *tris*(4-formyl phenyl)amine functionalized SBA-15, 2-aminophenol and CuCl₂ were taken in methanol in a round bottom flask. The molar ratio of the reactants was maintained at 1 : 2 : 2. Then the reaction mixture was refluxed for 4 h when the colour of the solution gradually darkened due to the *in situ* formation of CuO nanoparticles. The solid product was then isolated through filtration and washed repeatedly with methanol to remove any excess reactants. Finally, the brown coloured CuO nanoparticles immobilized over functionalized mesoporous silica (**nCuO-FMS**) were obtained after drying the product under vacuum.

Catalysis

In a typical catalytic reaction batch, 0.5 mmol iodo benzene, 1 mmol Se⁰ powder and 1 mmol KOH were taken together in a round bottom flask in the presence of 2.0 ml of DMSO as the solvent at 363 K and under nitrogen atmosphere. The reaction was initiated with the addition of 20 mg of **nCuO-FMS** as the catalyst into it. The reaction was allowed to continue for the desired time and the solid catalyst was separated from the reaction mixture by centrifugation and washed repeatedly to remove the organic product from it. Then, the product was extracted in ethyl acetate and washed thoroughly with brine solution and water for complete removal of the inorganic com-

ponents. The solid product was isolated through evaporation of the solvent and purified by column chromatography in a petroleum ether/ethyl acetate mixture. The isolated yield of the final product in pure form was obtained after solvent evaporation. The structure of the isolated product was characterized by ^1H and ^{13}C NMR spectroscopy in CDCl_3 and its percentage conversion, turnover frequency and turnover number were determined. To examine the recyclability of the catalyst, it was separated out from the reaction mixture after the completion of the reaction by centrifugation. The recovered catalyst was washed repeatedly with ethyl acetate, dried and used again for another catalytic cycle of Se-Se coupling.

Results and discussion

FT-IR spectra and thermal studies

The FT-IR spectra of SBA-15, 3-APTES functionalized SBA-15, trialdehyde loaded SBA-15 and **nCuO-FMS** have been recorded by the ATR technique with the powdered samples and the results are shown in Fig. 1. The spectrum of 3-APTES functionalized SBA-15 (Fig. 1(A)b) shows a broad band in the region of $3747\text{--}2929\text{ cm}^{-1}$ which may appear due to the presence of amine group and methylene moieties of the aminopropyl group.⁴⁸ For the trialdehyde loaded SBA-15 (Fig. 1(A)c), two additional peaks arise at 1643 cm^{-1} and 1698 cm^{-1} , which indicate the formation of azomethine bond and the presence of free aldehyde groups, respectively, in the material.⁴⁹ For **nCuO-FMS** (Fig. 1(A)d), the peak at 1698 cm^{-1} disappears indicating the complete conversion of free --CHO groups to C=N . The band at 1647 cm^{-1} indicates the retention of azomethine moiety. The peak at $\text{ca. } 1595\text{ cm}^{-1}$ may be due to the presence of aromatic C=C units which are present both in trialdehyde loaded SBA-15 and **nCuO-FMS**. For clarity, the region of interest for trialdehyde loaded SBA-15 and **nCuO-FMS** is shown in Fig. 1(B).

Thermogravimetric analyses have been carried out with the powder samples of SBA-15, 3-APTES functionalized SBA-15, trialdehyde loaded SBA-15 and **nCuO-FMS** in the temperature range of $303\text{--}1073\text{ K}$ to examine the thermal stability of the frameworks (Fig. 2). The high thermal stability of the silica support, SBA-15 (Fig. 2a), is quite clear from the curve, where only 4% weight loss takes place up to 1073 K , mostly due to the loss of adsorbed solvent and other molecules. Such high stability makes SBA-15 a potential candidate to act as the catalyst support. The thermal stabilities of the other samples can be ascertained from their corresponding TGA plots.^{50,51} All the organically modified materials (Fig. 2b–d) show a stepwise weight loss corresponding to the nature and amount of the functional groups present and the mass loss continues to take place at 1073 K . For all the samples, the first step of weight loss of *ca.* 3–4% takes place at around 373 K which can be attributed to the physisorbed water molecules. For the 3-APTES functionalized SBA-15 (Fig. 2a), there is another step of weight-loss corresponding to the removal of 3-aminopropyl moieties in the sample, between the temperature range of 530 and 820 K . The TGA profile of the trialdehyde loaded SBA-15 (Fig. 2c) also shows a similar trend, but the weight-loss is higher in this case due to the removal of 3-aminopropyl and the trialdehyde units. The catalyst, **nCuO-FMS** (Fig. 2d), loses more weight in this temperature region due to the removal of the 2-aminophenol units, in addition to the other organic functionalities, which plays an important role in stabilization of the CuO nanoparticles. It can also be seen from the plot that the material loses only *ca.* 5.5% of its weight up to 413 K and thus can be considered to be stable at least up to this temperature for its use as a catalyst. The percentage of functionalization in each step can be calculated from the data. The studies also give the amount of organic loading on the silica framework for each material. It can be calculated that 0.76 mmol of 3-APTES has been loaded on 1.0 g of SBA-15 and the amount of trialdehyde and 2-aminophenol is 0.18 mmol g^{-1} and 0.345 mmol g^{-1} , respectively.

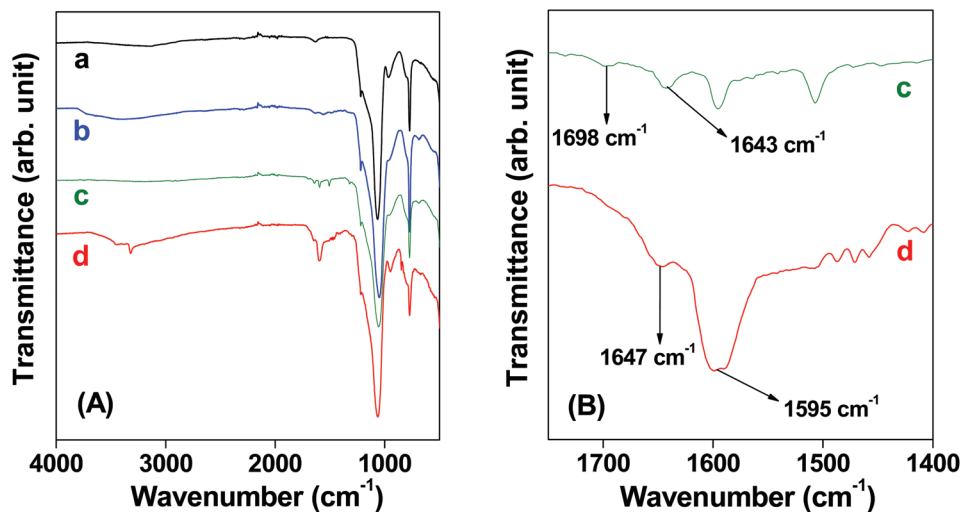


Fig. 1 (A) FT-IR spectra of (a) SBA-15, (b) 3-APTES functionalized SBA-15, (c) trialdehyde loaded SBA-15 and (d) **nCuO-FMS**; (B) magnified region of plot (c) and (d).

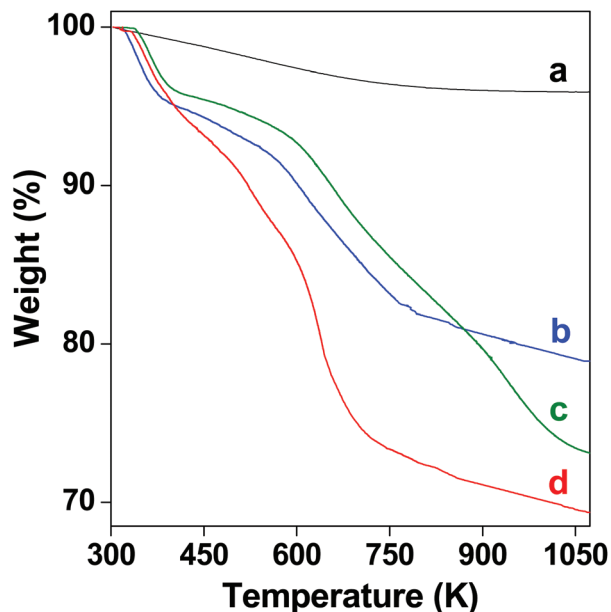


Fig. 2 Thermogravimetric study of (a) SBA-15, (b) 3-APTES functionalized SBA-15, (c) trialdehyde loaded SBA-15 and (d) nCuO-FMS.

Mesoporosity and microstructure

The powder X-ray diffraction patterns of SBA-15, 3-APTES functionalized SBA-15, trialdehyde loaded SBA-15 and nCuO-FMS are given in Fig. 3. All the samples are found to show a 2D-ordered hexagonal mesostructure which is evident from the presence of the three distinct diffraction peaks assigned to the

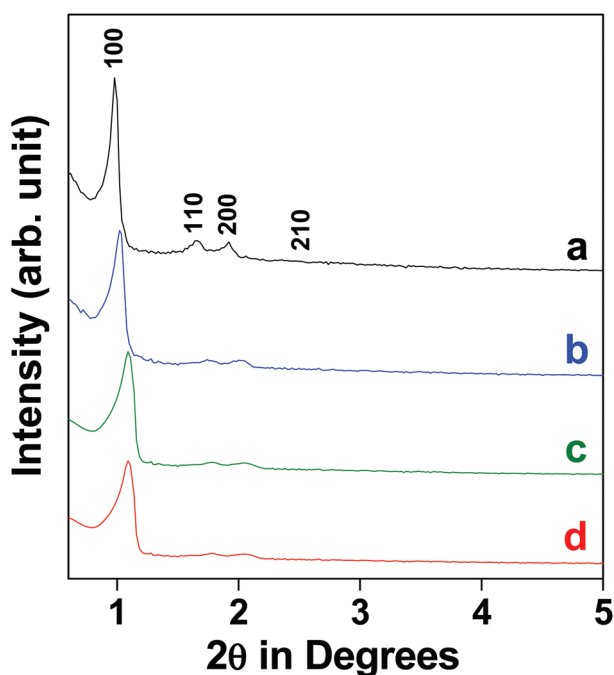


Fig. 3 Powder X-ray diffraction patterns of (a) SBA-15, (b) 3-APTES functionalized SBA-15, (c) trialdehyde loaded SBA-15 and (d) nCuO-FMS.

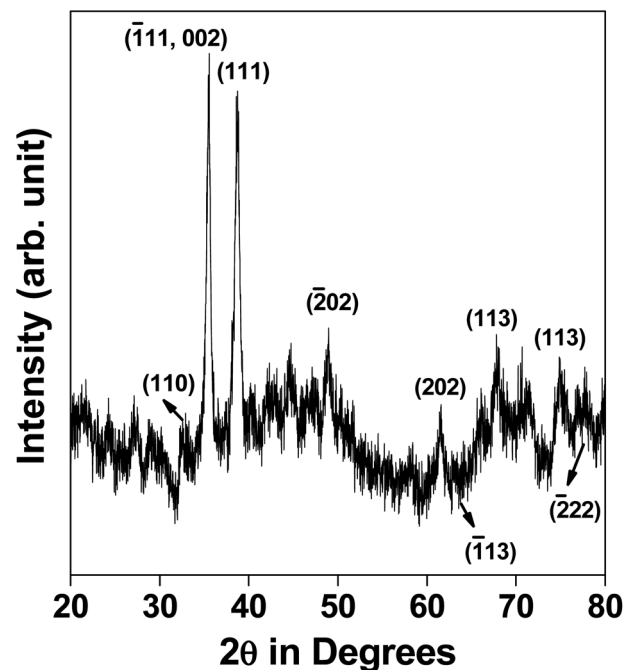


Fig. 4 Wide angle powder X-ray diffraction pattern of nCuO-FMS.

(100), (110) and (200) planes along with a very weak one for the (210) plane.^{52,53} However, the intensities of the peaks get lowered and the ordering of pores are affected in the materials with gradual functionalization. In addition, a reduction in pore size takes place which is indicated by the shifting of the peaks to higher 2θ values. The wide angle diffraction pattern of nCuO-FMS is shown in Fig. 4. Several diffraction peaks can be observed which are indexed in the figure and correspond to the characteristic planes of CuO.⁵⁴ Thus, it is conclusive from the figure that CuO nanoparticles have formed in the material.

Nitrogen physisorption analysis can be used to determine the total surface area, pore size and pore volume of nanoporous materials. Nitrogen adsorption/desorption isotherms have been measured at 77 K for SBA-15 and all the other samples obtained after each step of functionalization. From the isotherms shown in Fig. 5, it is possible to establish the mesoporous structures of SBA-15, 3-APTES functionalized SBA-15, trialdehyde loaded SBA-15 and nCuO-FMS. The BET surface area, pore volume and pore size of all the samples are presented in Table 1. By comparing these data, we can conclude that a gradual decrease in the BET surface area takes place with gradual functionalization over the mesoporous SBA-15 support. This is expected as the surfaces become occupied by various organic and inorganic moieties with every step of functionalization. The pattern of the isotherms for all the samples is type IV with a steep increase in the higher pressure region because of capillary condensation. This is a characteristic of the mesoporous nature of the materials.^{52,55} The isotherms of all the samples exhibit H1 type hysteresis loops between the P/P_0 values of 0.6 and 1.0 which is attributed to the presence of well-defined cylindrical pore channels⁵⁶ and

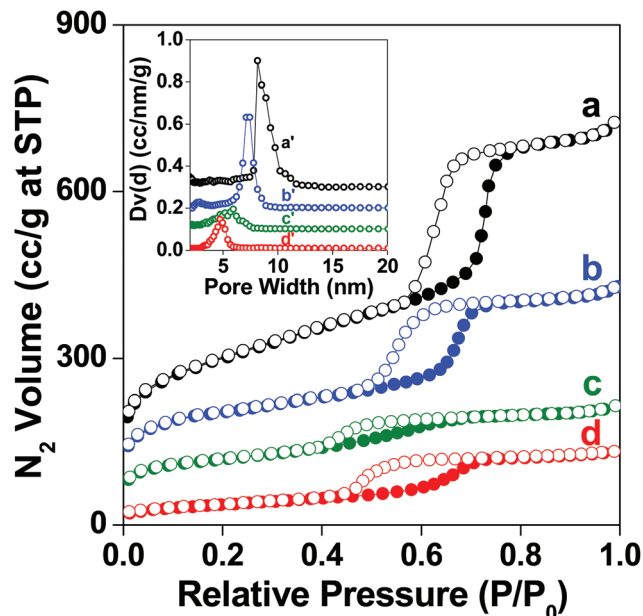


Fig. 5 Nitrogen adsorption-desorption isotherms of (a) SBA-15, (b) 3-APTES functionalized SBA-15, (c) trialdehyde loaded SBA-15 and (d) **nCuO-FMS**. For clarity, the Y-axis values have been increased by 100, 100 and 50 cc g⁻¹ for plots a, b and c, respectively. Adsorption points are marked by filled symbols and desorption points by empty symbols. Inset: NLDFT pore size distribution of (a') SBA-15, (b') 3-APTES functionalized SBA-15, (c') trialdehyde loaded SBA-15 and (d') **nCuO-FMS**. Y-axis values have been increased by 0.3, 0.25 and 0.15 cc nm⁻¹ g⁻¹, for plot (a'), (b') and (c'), respectively.

Table 1 Surface area, pore volume and pore size of the samples at various stages

Sample	BET surface area (m ² g ⁻¹)	Pore volume (cc g ⁻¹)	Pore size (nm)
(a) SBA-15	732	0.966	8.15
(b) 3-APTES functionalized SBA-15	366	0.652	7.45
(c) Trialdehyde loaded SBA-15	243	0.315	5.95
(d) nCuO-FMS	133	0.205	4.75

intercrystallite adsorption.⁵⁷ The average pore diameter of the starting mesoporous SBA-15 from the NLDFT model is 7.86 nm (inset of Fig. 5). The pore sizes of the functionalized materials follow a gradual descending trend as the incorporation of functional groups on the pore walls of the silica support inhibits the access of nitrogen gas molecules into the pores. A similar decreasing trend is also observed for the pore volume of the samples.

The transmission electron microscopic (TEM) images of SBA-15, trialdehyde loaded SBA-15 and **nCuO-FMS** are shown in Fig. 6. The image for SBA-15 (Fig. 6a) confirms the formation of a well-formed hexagonally arranged mesoporous structure as desirable for an appropriate solid support. Upon functionalization, the long range ordering of the pores is

decreased to some extent (Fig. 6b), however, the basic hexagonal structure is retained quite well. The TEM image of **nCuO-FMS** is shown in Fig. 6c. Spherical CuO particles with a diameter of *ca.* 6–7 nm could be seen dispersed throughout the matrix of mesoporous silica confirming the *in situ* generation of the nanoparticles. Thus, the powder X-ray diffraction, N₂ sorption experiments and TEM image analyses of the samples establish their microstructure and mesoporosity. In addition, the formation of CuO nanoparticles over the functionalized silica support can also be established from the studies. The amount of Cu²⁺ present in **nCuO-FMS** has been ascertained from the atomic absorption spectrophotometric study. It has been found that 1.0 g of **nCuO-FMS** contains 2.096 × 10⁻⁴ mol or 13.32 mg of Cu²⁺.

Solid state NMR studies

The chemical environments around the silicon atom in the synthesized materials have been studied by ²⁹Si MAS NMR and the results are given in Fig. 7. For SBA-15, peaks are obtained at *ca.* -111.65 and -103.17 ppm (Fig. 7a) which can be assigned to the Q⁴ and Q³ silica centers of the Si(OSi)_n(OH)_{4-n} units. For the 3-APTES functionalized SBA-15 (Fig. 7b), apart from the peaks for Q₄ and Q₃ silica species, additional peaks appear at -67.0 and -58.06 ppm due to the incorporation of the aminopropyl group in the matrix. The chemical environment of the starting silica support changes due to such addition of aminopropyl groups and the new peaks can be attributed to the T³ ((SiO)₃Si-R-Si(OSi)₃) and T² ((HO)₂(OSi)Si-R-Si(OSi)₂(OH)) species,^{58,59} respectively. The spectra for the other two samples, trialdehyde loaded SBA-15 and **nCuO-FMS** (Fig. 7c and d, respectively), show similar patterns to 3-APTES modified SBA-15 which indicates the formation and retention of imine bonds in both the samples. A marginal shifting of the peak position is observed for **nCuO-FMS** (Fig. 7d) due to the formation of CuO nanoparticles which are stabilized by the N and O groups of the functionalized silica framework through noncovalent interactions.^{60,61}

¹³C CP MAS NMR studies have been performed with the materials having organic contents and the spectra are shown in Fig. 8. The spectrum for 3-APTES functionalized SBA-15 (Fig. 8a) shows peaks at 9.71, 22.39, 29.17 and 42.86 ppm. The signal at 42.86 ppm may be attributed to the carbon adjacent to the amine group, the signals at 29.17 and 22.39 ppm may appear due to the α and β carbon atoms with respect to the -NH₂ group and the signal at 9.71 ppm may be attributed to the other aliphatic carbon atoms. For trialdehyde loaded SBA-15 (Fig. 8b), several new peaks emerge at 10.47, 21.84, 42.86 and 63.98 ppm for the aliphatic carbon atoms and at 151, 164.84 and 128.95 ppm for the aromatic carbon atoms. Two characteristic peaks at 183.72 and 199.78 ppm appear due to the formation of the C=N bond (imine bond) and the free aldehyde group, respectively. From this spectrum, we can conclude that Schiff base reaction has taken place between the trialdehyde and 3-APTES loaded silica and at the same time residual free aldehyde groups are also present. For **nCuO-FMS** (Fig. 8c), the peaks corresponding to the aliphatic and aro-

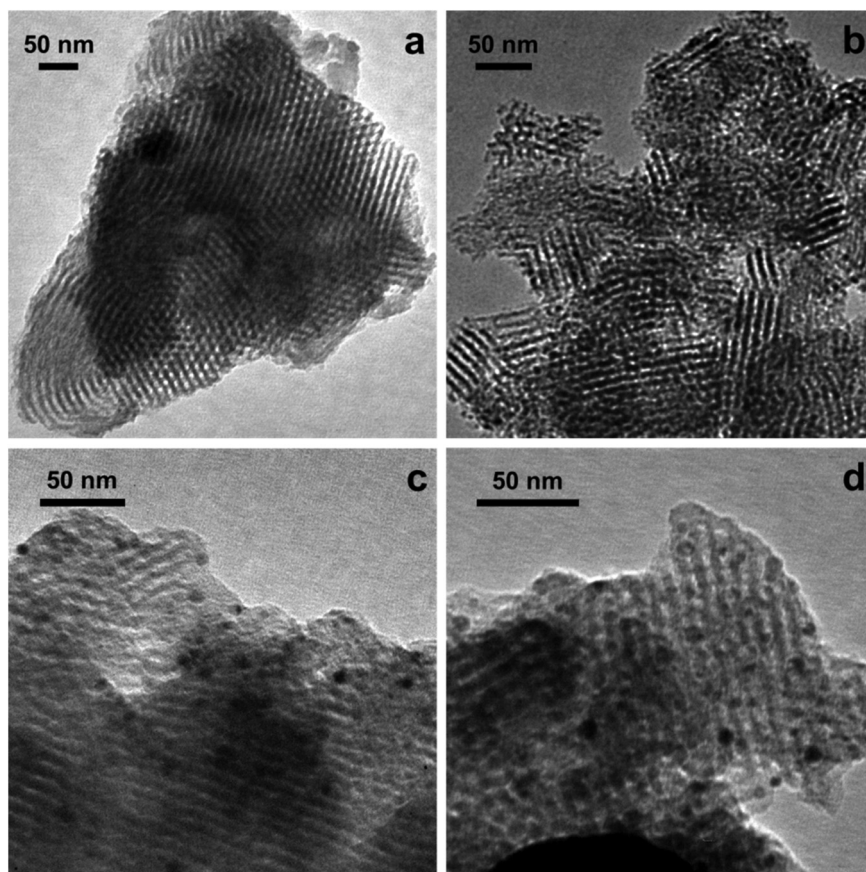


Fig. 6 TEM images of (a) SBA-15, (b) trialdehyde loaded SBA-15, (c) nCuO-FMS and (d) reused nCuO-FMS.

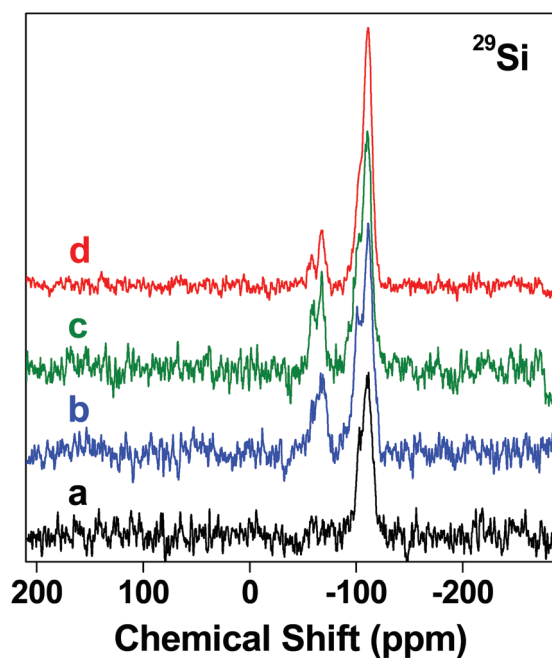


Fig. 7 Solid state ^{29}Si MAS NMR spectra of (a) SBA-15, (b) 3-APTES functionalized SBA-15, (c) trialdehyde loaded SBA-15 and (d) nCuO-FMS.

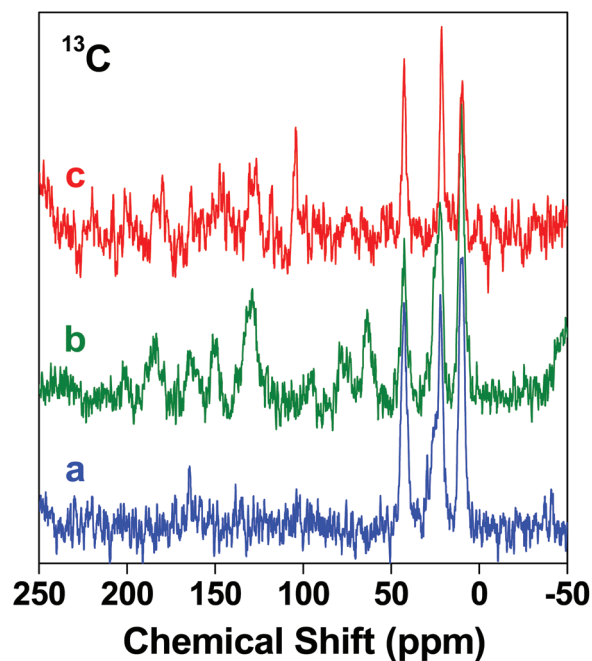


Fig. 8 Solid state ^{13}C CP-MAS NMR spectra of (a) 3-APTES functionalized SBA-15, (b) trialdehyde loaded SBA-15 and (c) nCuO-FMS.

matic regions are found to remain almost intact. However, two new peaks appear at 147.76 and 163.67 ppm which may be attributed to the aromatic carbon attached to the phenolic -OH group and imine bond formation, respectively. The peak at 163.67 ppm confirms the complete conversion of the residual -CHO groups of trialdehyde to C=N after condensation with 2-aminophenol.

XPS analysis

The wide scan and fitted XPS spectra of nCuO-FMS are shown in Fig. 9. The survey spectrum (Fig. 9a) reveals the presence of Si, C, O, N and Cu in the material, in agreement with the expected elemental distribution. The Cu(2p) spectra (Fig. 9b)

reveal two states with binding energies of 934.6 eV and 932.1 eV and assigned to the Cu 2p_{3/2} states, for Cu(II), in CuO and reduced Cu, respectively; the lower binding energy species can be attributed to the reduction of the Cu(II) species during analysis.^{62,63} Fig. 9c and d show the multiple states of oxygen and carbon present within the material. The peak at 532.7 eV is assigned primarily to Si-O bonds, although the presence of carbon-oxygen functions at this energy also cannot be discounted. The peaks at 531.1 and 533.8 eV can be ascribed to inorganic (Cu-O)⁶⁴ and organic oxygen, respectively. The binding energies of different types of carbon present in the sample are illustrated in Fig. 9d. Four distinct peaks appear at 284.3, 284.7, 286 and 287.1 eV and can be attributed to the

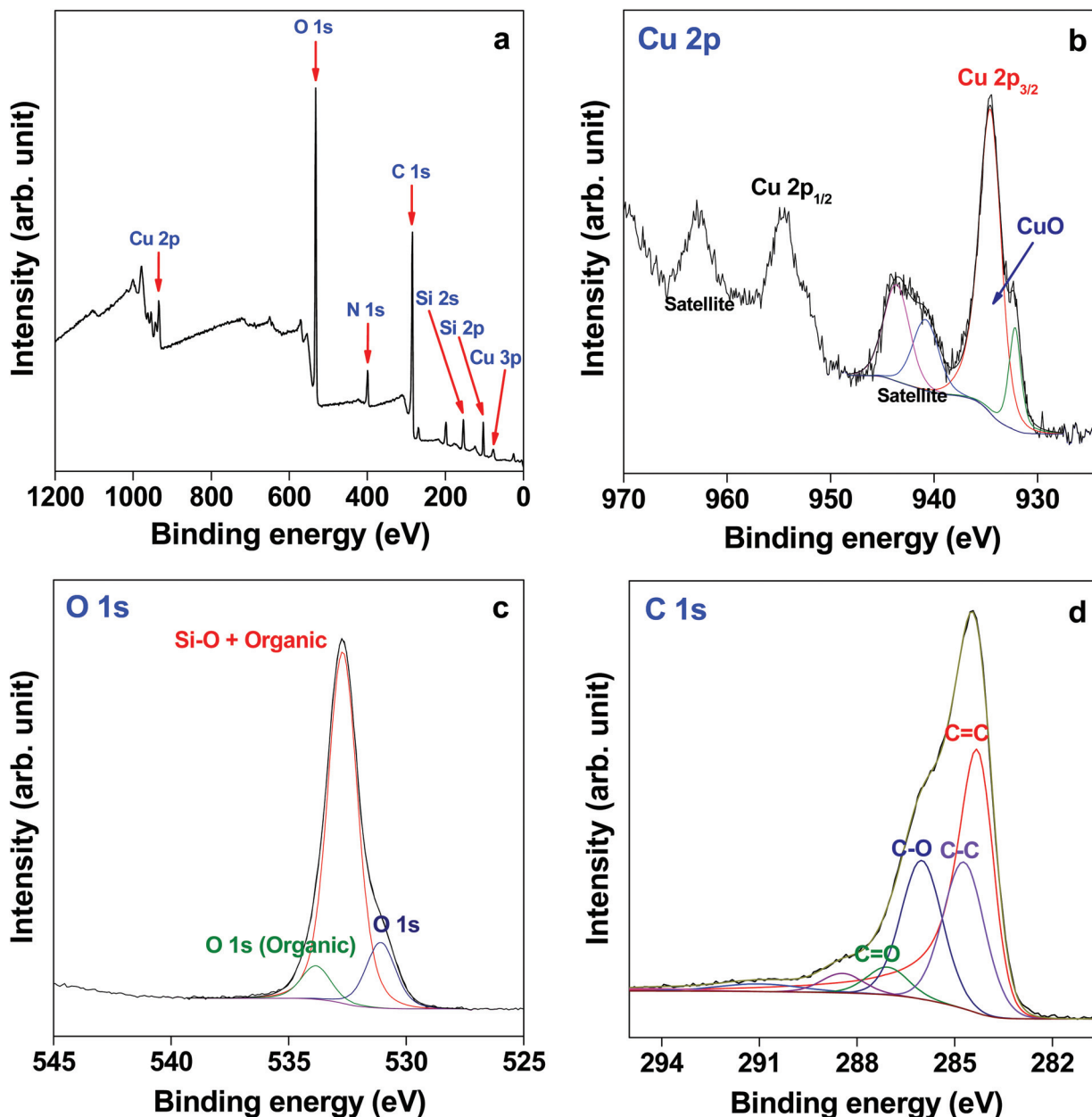


Fig. 9 XPS spectra of nCuO-FMS (a) wide scan, (b) Cu 2p core-level, (c) O 1s core-level and (d) C 1s core-level.

presence of the C=C, C-C, C-O and C=O species in **nCuO-FMS**, respectively.⁶⁵

Catalytic studies

The catalytic efficiency of **nCuO-FMS** has been studied for Se-Se coupling reaction under different reaction conditions (Table 2). To begin with, different amounts of **nCuO-FMS** are used to study the reaction between iodobenzene (0.5 mmol), Se⁰ powder (1.0 mmol) and KOH (1.0 mmol) in 2.0 ml of dimethyl sulphoxide (DMSO) at 363 K under nitrogen atmosphere to ascertain the maximum yield. The product obtained is 1,2-diphenyl diselenide (**3a**). The reaction does not produce significant amounts of the product when 1 mg of **nCuO-FMS** is used for the catalytic reaction (entry 1). With a gradual increase in the amount of the catalyst to 2, 5 and 10 mg (entries 2–4), the yield is found to increase slowly to 25, 46 and 64%, respectively. When the amount of **nCuO-FMS** is increased to 20 mg, the yield reaches 78% (entry 5), and this is the maximum value at the given temperature. When the amount of catalyst is increased further to 30 mg, product formation is not affected much and the yield is 79% (entry 6). Thus, it can be established that 20 mg of **nCuO-FMS** is sufficient for achieving the best yield of **3a** for this optimization reaction under the specified conditions. In the next step, the base is altered; KOH is replaced by NaOH and the yield is found to be lower at 67% (entry 7). Then the reaction is carried out by changing the solvent to dimethyl formamide (DMF) and acetonitrile (CH₃CN), and the yields reduce to 73 and 63% (entries 8 and 9), respectively. Finally, the reaction is performed at different temperatures. Increasing the temperature to 373 K does not improve the product yield (78% yield, entry 10), while by decreasing the temperature to 333 K a lower yield (55%, entry 11) is obtained.

To study the time dependent conversion of iodobenzene to 1,2-diphenyl diselenide, the reaction in DMSO solvent is then

carried out for different time periods (Table 3). It can be seen that the conversion increases marginally as the reaction time is increased from 3 h to 6, 9 and 12 h. After 12 h, the isolated yield obtained is 83% (entry 4) which is a little better than the 78% yield that is obtained within 3 h (entry 1) of the reaction. So, it can be concluded that if the reaction time is increased the yields do not increase significantly, and thus in the present study, the reaction time has been optimized at 3 h. However, it should be noted that isolated yields are always lower than the actual conversion in a reaction since some amount of the product is lost during the process of work-up, isolation and purification of the final reaction mixture.

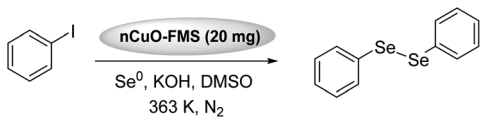
After determining the optimized reaction conditions, the conversions have been carried out using various substituted iodobenzenes to produce the corresponding 1,2-diphenyl diselenide derivatives (Table 4). When 4-methyl iodobenzene and 3-methyl iodobenzene are used, the products, 1,2-di-*p*-tolyl-diselane (**3b**) and 1,2-di-*m*-tolyl-diselane (**3c**), are obtained with very good yields of 77 and 75%, respectively. To explore the scope of substrate for the reactions, substituted iodobenzenes with different groups (–F, –Cl, –Br, –CF₃) have been studied. 4-Fluoro iodobenzene reacted to form 1,2-bis(4-fluorophenyl) diselenide (**3d**) with a 74% yield, 4-chloro iodobenzene formed 1,2-bis(4-chlorophenyl)diselenide (**3e**) with a 76% yield and 4-bromo iodobenzene formed 1,2-bis(4-bromophenyl)diselenide (**3f**) with a 75% yield. 3-Trifluoromethyl iodobenzene gives 1,2-bis(3-(trifluoromethyl)phenyl)diselenide (**3g**) as the product with a 72% yield. A heterocyclic iodo compound, 2-iodothiophene, has also been used for the study. The product, 1,2-di(thiophen-2-yl)diselenide (**3h**), is obtained and the yield is 73%. Thus, it is observed that iodobenzene with no substituent gives the finest result among the substrates.

The ¹H NMR, ¹³C NMR, ⁷⁷Se NMR and mass spectra are given in the ESI† with the structure of the corresponding compounds.

Table 2 Optimization of the catalytic conditions^a


Entry	nCuO-FMS (in mg)	Base	Temperature (K)	Solvent	Isolated yield ^b (%)	TON	TOF
1	1	KOH	363	DMSO	Trace	—	—
2	2	KOH	363	DMSO	25	29.82	9.940
3	5	KOH	363	DMSO	46	54.87	18.288
4	10	KOH	363	DMSO	64	76.35	25.445
5	20	KOH	363	DMSO	78	93.03	31.011
6	30	KOH	363	DMSO	79	94.23	31.409
7	20	NaOH	363	DMSO	67	79.91	26.638
8	20	KOH	363	DMF	73	87.07	29.023
9	20	KOH	363	CH ₃ CN	63	75.14	25.05
10	20	KOH	373	DMSO	78	93.03	31.011
11	20	KOH	333	DMSO	55	65.60	21.867

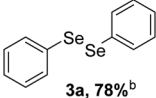
^a All the reactions are carried out for 3 h with 0.5 mmol of substrate, 1.0 mmol Se⁰ and 1.0 mmol of base. ^b Yields determined by NMR spectroscopy.

Table 3 Time dependent conversion of iodobenzene in the catalytic Se–Se coupling reaction^a


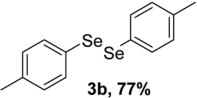
Entry	Time (h)	Isolated yield ^b (%)	TON	TOF
1	3	78	93.03	31.01
2	6	80	95.42	31.81
3	9	81	96.61	32.20
4	12	83	99.00	33.00

^a The reactions have been carried out in 2 ml of DMSO as the solvent with 0.5 mmol of iodobenzene, 1.0 mmol of Se⁰ powder and 1.0 mmol of KOH, at 363 K using 20 mg of **nCuO-FMS** as the catalyst. ^b Yields determined by NMR spectroscopy.

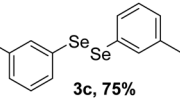
Table 4 Catalytic Se–Se coupling reactions using different substrates^a




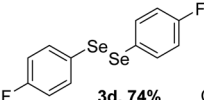
3a, 78%^b



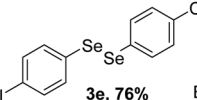
3b, 77%



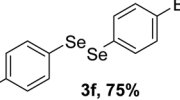
3c, 75%



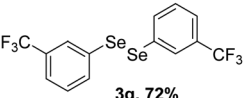
3d, 74%



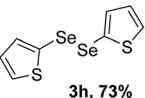
3e, 76%



3f, 75%



3g, 72%



3h, 73%

Entry	R/substrate	Isolated yield ^b (%)	TON	TOF
3a	—	78	93.03	31.01
3b	4-CH ₃	77	91.84	30.61
3c	3-CH ₃	75	89.46	29.82
3d	4-F	74	88.26	29.42
3e	4-Cl	76	90.65	30.22
3f	4-Br	75	89.46	29.82
3g	3-CF ₃	72	85.88	28.63
3h	2-Iodothiophene	73	87.07	29.02

^a The reactions have been carried out for 3 h in 2 ml of DMSO as the solvent with 0.5 mmol of the respective substrates, 1.0 mmol of Se⁰ powder and 1.0 mmol of KOH at 363 K using 20 mg of **nCuO-FMS** as the catalyst. ^b Yields determined by NMR spectroscopy.

Recyclability

The ability to recycle is the most attractive feature of a heterogeneous catalyst. In this work, to study the recyclability of **nCuO-FMS** in Se–Se coupling, the reaction of iodobenzene as

the substrate has been studied under the optimized conditions. In each cycle, 0.5 mmol iodobenzene, 1.0 mmol Se⁰ powder and 1.0 mmol KOH are taken in 2.0 ml of DMSO and the reaction is carried out at 363 K under nitrogen atmosphere for 3 h. Then the catalyst is recovered, regenerated and reused in the subsequent run. The conversion (%) against the number of reaction cycles for the coupling is given in Fig. 10. The percentage conversions for five cycles are 78, 78, 75, 70 and 68%, respectively. It can be seen that the efficiency of the catalyst remains more or less the same in the first two cycles. After that there is a marginal drop in the percentage of conversion in each step and after five cycles it is 68%. The gradual drop in conversion from the first to the fifth cycle may be attributed to the partial damage of the mesoporous structure of the catalyst when it remains in the matrix of the catalytic system for a prolonged period during the reactions. Thus, it can be inferred that the catalyst has a good recycling efficiency. The TEM image of recycled **nCuO-FMS** is illustrated in Fig. 6d. It shows that the porous structure of the mesoporous silica matrix is retained even after the catalytic performance and the immobilization of the CuO nanoparticles over it also remains intact. In addition, the surface area of the recycled catalyst is also not reduced to a large extent which adds to the reusability of the material as a catalyst.

Mechanism

A plausible mechanism⁶⁶ can be proposed for the Se–Se coupling reaction and it is shown in Scheme 2. In the presence of a base, selenium gives selenide or selenite anion and in a super basic DMSO/KOH medium a reductive dimsly species is produced. The dimsly species is responsible for the formation of the desired diselenide anion. This preformed anion is considered to be the active species involved in the catalytic cycle. The formation of species **a** and **b** takes place by the ligand exchange with the diselenide anion and may further generate complex **c**. Then, species **c** may undergo reductive elimination *via* the formation of the initial coupling product **d** and the CuO nanoparticles in **nCuO-FMS** are regenerated. Then **d** probably reacts with another unit of **b** to form a new complex **e**. Finally, the desired diselenide compound **f** is formed by another step of reductive elimination and the other unit of CuO nanoparticles of **nCuO-FMS** could be regenerated. The CuO nanoparticles thus recovered can be used in the next catalytic cycle.

The amount of copper present in 1 g of **nCuO-FMS** as determined by AAS study is 2.096×10^{-4} mol or 13.32 mg of Cu. We have optimized the amount of catalyst at 20 mg for all the reactions, which means 0.041 mmol or 0.266 mg of Cu is used in each cycle to catalyse 1 mmol of substrate. On the other hand, when commercially available CuO nanoparticles have been used,^{40,44} the amounts of Cu used for the catalysis have been found to be 3.2–6.4 mg of Cu for 1 mmol of substrate. Clearly, the amount of active copper centers in **nCuO-FMS** is much less compared to that in the reported studies. This is the advantage of a heterogeneous framework where more active sites are exposed on the surface of the catalyst and thus a very small

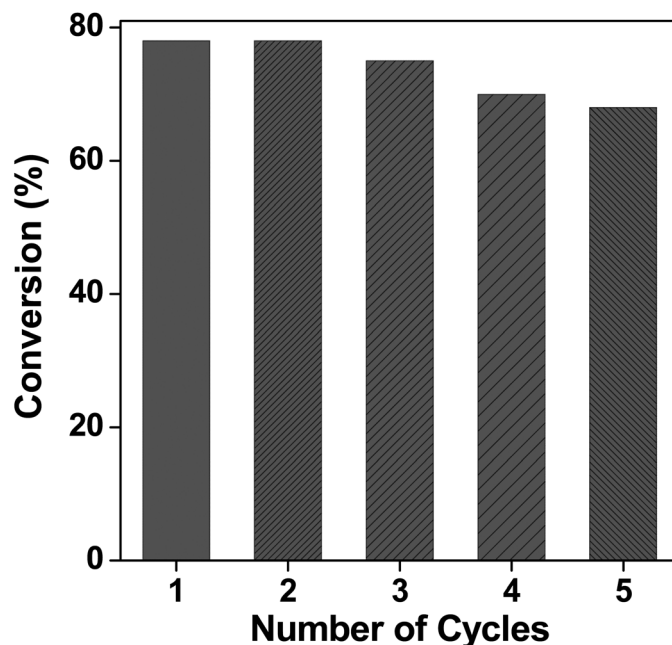
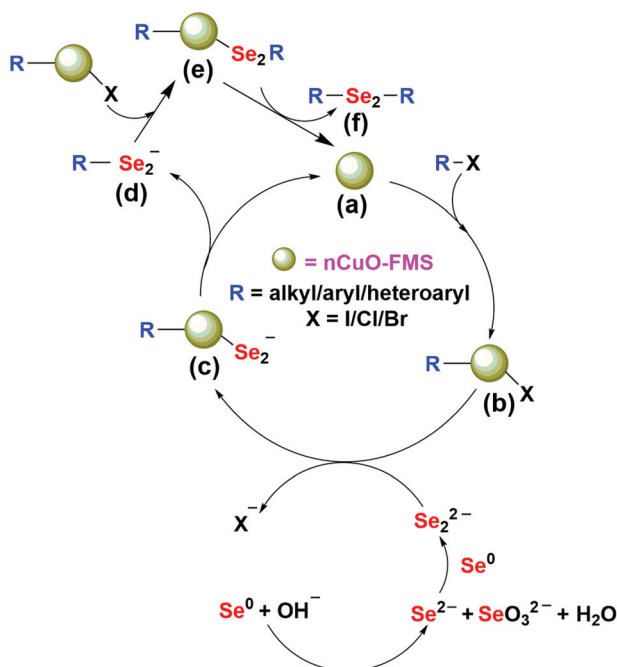


Fig. 10 Recycling efficiency of nCuO-FMS for Se-Se coupling using iodobenzene.



Scheme 2 Plausible mechanism for organo diselenide synthesis.

amount of the catalyst is sufficient to catalyse the reactions. This is also beneficial from an environmental point of view. In addition, the CuO nanopowder based catalytic systems reported in the previous studies^{40,44} do not provide any data on the reusability of the catalyst. In this respect, the supported heterogeneous catalyst reported in this work can be recycled several times and is thus more economical compared to as-purchased CuO nanoparticle based catalytic systems.

Conclusions

In this article, we have synthesized a mesoporous silica based catalyst with immobilized CuO nanoparticles **nCuO-FMS**, using a facile synthetic route. The generation of CuO nanoparticles takes place *in situ* in the presence of 2-amino-phenol, which also acts as a stabilizing support to the metal oxide particles. The silica support, SBA-15, and all the other subsequent organically functionalized frameworks, including the catalyst, have been characterized thoroughly to establish their structure. These CuO nanoparticles containing porous silica with good specific surface area are found to catalyze the Se-Se coupling reaction to produce symmetrical diselenides with high yields. Thus, it provides a simple and efficient method for the preparation of diselenides through the cross-coupling reaction between selenium and aryl iodides. The process is chemoselective and can be used to prepare a wide range of substituted symmetrical diselenides containing *e.g.* methoxy, carboxylate, hydroxyl, amino, aldehyde and bromo groups. The superior activity of the catalyst can be attributed to the nanoscale dimension of the CuO particles and the high surface area of the silica matrix which predisposes the substrates better at the catalytically active metal centres. The catalyst is cheaper than the commercially available CuO nanopowder and due to its heterogeneous nature it can be economically used for several reaction cycles.

Conflicts of interest

There are no conflicts to declare.

Acknowledgements

MN thanks the DST-SERB, India (SB/FT/CS-004/2014 dated 27/06/2014) and the WB-DST, India (ST/P/S&T/15G-20/2018) for financial support. The authors are thankful to N. Pradhan and J. Guin of the Indian Association for the Cultivation of Science for providing TEM and GC-MS facilities and G. Ghosh of Visva-Bharati for AAS studies.

References

- 1 K. C. Gupta, A. K. Sutar and C.-C. Lin, *Coord. Chem. Rev.*, 2009, **253**, 1926.
- 2 D. R. Godhani, H. D. Nakum, D. K. Parmar, J. P. Mehta and N. C. Desai, *J. Mol. Catal. A: Chem.*, 2017, **426**, 223.
- 3 M. Trueba and S. P. Trasatti, *Eur. J. Inorg. Chem.*, 2005, **17**, 3393.
- 4 E. L. Margelefsky, R. K. Zeidan and M. E. Davis, *Chem. Soc. Rev.*, 2008, **37**, 1118.
- 5 A. Zarnegaryan, M. Moghadam, S. Tangestaninejad, V. Mirkhani and I. Mohammadpoor-Baltork, *New J. Chem.*, 2016, **40**, 2280.
- 6 Y. Zhang, A. Wang and T. Zhang, *Chem. Commun.*, 2010, **46**, 862.
- 7 J. M. Planeix, N. Coustel, B. Coq, V. Brotons, P. S. Kumbhar, R. Dutartre, P. Geneste, P. Bernier and P. M. Ajayan, *J. Am. Chem. Soc.*, 1994, **116**, 7935.
- 8 A. Dhakshinamoorthy and H. Garcia, *Chem. Soc. Rev.*, 2014, **43**, 5750.
- 9 S. Zhou, M. Johnson and J. G. C. Veinot, *Chem. Commun.*, 2010, **46**, 2411.
- 10 H. Noh, Y. Cui, A. W. Peters, D. R. Pahls, M. A. Ortuñ, N. A. Vermeulen, C. J. Cramer, L. Gagliardi, J. T. Hupp and O. K. Farha, *J. Am. Chem. Soc.*, 2016, **138**, 14720.
- 11 C. M. A. Parlett, K. Wilson and A. F. Lee, *Chem. Soc. Rev.*, 2013, **42**, 3876.
- 12 T. Toyao, K. Miyahara, M. Fujiwaki, T.-H. Kim, S. Dohshi, Y. Horiuchi and M. Matsuoka, *J. Phys. Chem. C*, 2015, **119**, 8131.
- 13 R. M. Rioux, H. Song, J. D. Hoefelmeyer, P. Yang and G. A. Somorjai, *J. Phys. Chem. B*, 2005, **109**, 2192.
- 14 C. Xu, X. Wang, J. Zhu, X. Yang and L. Lu, *J. Mater. Chem.*, 2008, **18**, 5625.
- 15 G. B. Shul'pin, *Catalysts*, 2016, **6**, 50.
- 16 K. C. Gupta and A. K. Sutar, *Coord. Chem. Rev.*, 2008, **252**, 1420.
- 17 M. B. Thathagar, J. Beckers and G. Rothenberg, *J. Am. Chem. Soc.*, 2002, **124**, 11858.
- 18 T. Kamal, *Polym. Test.*, 2019, **77**, 105896.
- 19 L. Xu, J. Zhang, Z. Li, Q. Ma, Y. Wang, F. Cui and T. Cui, *New J. Chem.*, 2019, **43**, 520.
- 20 X. Xiong, C. You, Z. Liu, A. M. Asiri and X. Sun, *ACS Sustainable Chem. Eng.*, 2018, **6**, 2883.
- 21 S. Vázquez-Céspedes, K. M. Chepiga, N. Möller, A. H. Schäfer and F. Glorius, *ACS Catal.*, 2016, **6**, 5954.
- 22 N. K. Ojha, G. V. Zyryanov, A. Majee, V. N. Charushin, O. N. Chupakhin and S. Santra, *Coord. Chem. Rev.*, 2017, **353**, 1.
- 23 A. Fihri, M. Bouhrara, B. Nekoueishahraki, J.-M. Basset and V. Polshettiwar, *Chem. Soc. Rev.*, 2011, **40**, 5181.
- 24 G. Mugesh, W. W. du Mont and H. Sies, *Chem. Rev.*, 2001, **101**, 2125.
- 25 C. W. Nogueira and J. B. T. Rocha, *Arch. Toxicol.*, 2011, **85**, 1313.
- 26 K. Didehban, E. Vessally, A. Hosseinian, L. Edjlali and E. S. Khosroshahi, *RSC Adv.*, 2018, **8**, 291.
- 27 V. Nascimento, E. E. Alberto, D. W. Tondo, D. Dambrowski, M. R. Detty, F. Nome and A. L. Braga, *J. Am. Chem. Soc.*, 2012, **134**, 138.
- 28 D. M. Freudentahl, S. Santoro, S. A. Shahzad, C. Santi and T. Wirth, *Angew. Chem., Int. Ed.*, 2009, **48**, 8409.
- 29 A. Gucchait, N. Joardar, P. K. Parida, P. Roy, N. Mukherjee, A. Dutta, R. Yesuvadian, S. P. SinhaBabu, K. Jana and A. K. Misra, *Eur. J. Med. Chem.*, 2018, **143**, 598.
- 30 D. Plano, Y. Baquedano, D. Moreno-Mateos, M. Font, A. Jiménez-Ruiz, J. A. Palop and C. Sanmartín, *Eur. J. Med. Chem.*, 2011, **46**, 3315.
- 31 P. G. Geiger, F. Lin and A. W. Girotti, *Free Radical Biol. Med.*, 1993, **14**, 251.
- 32 E. E. Alberto, V. Nascimento and A. L. Braga, *J. Braz. Chem. Soc.*, 2010, **21**, 2032.
- 33 C. W. Nogueira, G. Zeni and J. B. T. Rocha, *Chem. Rev.*, 2004, **104**, 6255.
- 34 E. R. T. Tiekink, *Dalton Trans.*, 2012, **41**, 6390.
- 35 G. I. Dzhardimalieva and I. E. Uflyand, *J. Coord. Chem.*, 2019, **72**, 1.
- 36 T. Manna and A. K. Misra, *SynOpen*, 2018, **2**, 229.
- 37 D. Tanini, A. Degl'Innocenti and A. Capperucci, *Eur. J. Org. Chem.*, 2015, 357.
- 38 M. A. Rizvi, S. Guru, T. Naqvi, M. Kumar, N. Kumbhar, S. Akhoun, S. Banday, S. K. Singh, S. Bhushan, G. M. Peerzada and B. A. Shah, *Bioorg. Med. Chem. Lett.*, 2014, **24**, 3440.
- 39 Z. Li, F. Ke, H. Deng, H. Xu, H. Xiang and X. Zhou, *Org. Biomol. Chem.*, 2013, **11**, 2943.
- 40 G. V. Botteselle, M. Godoi, F. Z. Galetto, L. Bettanin, D. Singh, O. E. Rodrigues and A. L. Braga, *J. Mol. Catal. A: Chem.*, 2012, **365**, 186.
- 41 A. Krief, W. Dumont and C. Delmotte, *Angew. Chem., Int. Ed.*, 2000, **39**, 1669.
- 42 F. Tian, Z. Yu and S. Lu, *J. Org. Chem.*, 2004, **69**, 4520.
- 43 P. Salama and C. Bernard, *Tetrahedron Lett.*, 1998, **39**, 745.
- 44 D. Singh, A. M. Deobald, L. R. S. Camargo, G. Tabarelli, O. E. D. Rodrigues and A. L. Braga, *Org. Lett.*, 2010, **12**, 3288.
- 45 D. Zhao, J. Feng, Q. Huo, N. Melosh, G. H. Fredrickson, B. F. Chmelka and G. D. Stucky, *Science*, 1998, **279**, 548.
- 46 T. Mallegol, S. Gmouh, M. A. A. Meziane, M. B.-Desce and O. Mongin, *Synthesis*, 2005, 1771.
- 47 T. Das, H. Uyama and M. Nandi, *New J. Chem.*, 2018, **42**, 6416.

- 48 D. Singha, T. Das, L. Satyanarayana, P. Roy and M. Nandi, *New J. Chem.*, 2019, **43**, 15563.
- 49 K. Sarkar, K. Dhara, M. Nandi, P. Roy, A. Bhaumik and P. Banerjee, *Adv. Funct. Mater.*, 2009, **19**, 223.
- 50 C. Sarkar, P. Koley, I. Shown, J. Lee, Y.-F. Liao, K. An, J. Tardio, L. Nakka, K.-H. Chen and J. Mondal, *ACS Sustainable Chem. Eng.*, 2019, **7**, 10349.
- 51 S. K. Verma and V. K. Singh, *J. Coord. Chem.*, 2015, **68**, 1072.
- 52 A. P. Wight and M. E. Davis, *Chem. Rev.*, 2002, **102**, 3589.
- 53 O. Olkhovik and M. Jaroniec, *J. Am. Chem. Soc.*, 2005, **127**, 60.
- 54 V. V. T. Padil and M. Černík, *Int. J. Nanomed.*, 2013, **8**, 889.
- 55 A. Stein, *Adv. Mater.*, 2003, **15**, 763.
- 56 M. Thommes, K. Kaneko, A. V. Neimark, J. P. Olivier, F. Rodriguez-Reinoso, J. Rouquerol and K. S. Sing, *Pure Appl. Chem.*, 2015, **87**, 1051.
- 57 T. Tanev and T. J. Pinnavaia, *Science*, 1996, **271**, 1267.
- 58 S. Inagaki, S. Guan, Y. Fukushima, T. Ohsuna and O. Terasaki, *J. Am. Chem. Soc.*, 1999, **121**, 9611.
- 59 S. Inagaki, S. Guan, T. Ohsuna and O. Terasaki, *Nature*, 2002, **416**, 304.
- 60 C. Sarkar, S. Pendem, A. Shrotri, D. Q. Dao, P. P. T. Mai, T. N. Ngoc, D. R. Chandaka, T. V. Rao, Q. T. Trinh, M. P. Sherburne and J. Mondal, *ACS Appl. Mater. Interfaces*, 2019, **11**, 11722.
- 61 S. C. Shit, R. Singuru, S. Pollastri, B. Joseph, B. S. Rao, N. Lingaiah and J. Mondal, *Catal. Sci. Technol.*, 2018, **8**, 2195.
- 62 L. Xu, J. Zhang, Z. Li, Q. Ma, Y. Wang, F. Cui and T. Cui, *New J. Chem.*, 2019, **43**, 520.
- 63 T. L. Freeman, S. D. Evans and A. Ulman, *Thin Solid Films*, 1994, **244**, 784.
- 64 H. Wang, J.-Z. Xu, J.-J. Zhu and H.-Y. Chen, *J. Cryst. Growth*, 2002, **244**, 88.
- 65 Y. Liu, L. Ma, D. Zhang, G. Han and Y. Chang, *RSC Adv.*, 2017, **7**, 12027.
- 66 V. P. Reddy, A. V. Kumar, K. Swapna and K. R. Rao, *Org. Lett.*, 2009, **11**, 951.